Research Article | Vol. 29, No. 12 / 7 June 2021 / Optics Express 18070
Optics EXPRESS

Band engineering method to create Dirac cones of accidental degeneracy in general photonic crystals without symmetry

HONGCHEN CHU,[1] YANG ZHANG,[1] JIE LUO,[2] CHANGQING XU,[3] XIANG XIONG,[1] RUWEN PENG,[1] MU WANG,[1] AND YUN LAI[1,*]

[1]MOE Key Laboratory of Modern Acoustics, National Laboratory of Solid State Microstructures, School of Physics, and Collaborative Innovation Center of Advanced Microstructures, Nanjing University, Nanjing 210093, China
[2]School of Physical Science and Technology, Soochow University, Suzhou 215006, China
[3]Division of Computer, Electrical and Mathematical Science and Engineering, King Abdullah University of Science and Technology (KAUST), Thuwal 23955-6900, Saudi Arabia
*laiyun@nju.edu.cn

Abstract: Symmetry usually plays a key role in the formation of the Dirac cone in the band structure of triangular or hexagonal systems. In this work, we demonstrate a systematic method to create Dirac cones of accidental degeneracy in general photonic crystals without symmetry. With this method, a band gap can be closed gradually through a series of modification to the unit structure based on the eigenfields of the band edges, and consequently a Dirac point is formed with Dirac conical dispersions in its vicinity. The validity of this approach is demonstrated by three examples. We further show that the Dirac cones of accidental degeneracy have the same properties as the symmetry-induced Dirac cones, such as finite group velocity and pseudo-diffusive transmission. Our finding opens a route for the engineering of accidental degeneracy in general photonic crystals beyond the scope of high-symmetry ones.

1. Introduction

Symmetry plays a significant role in forming novel band diagrams, which can induce intricate characteristics in condensed matter physics [1–4] and periodic systems of classical waves like metamaterials [5–7], photonic crystals [8–16] and sonic crystals [17–20], etc. Especially, the Dirac cone and linear dispersion relations around the K and K' points in the Brillouin zone of the triangular or hexagonal systems have recently attracted immense attention. Due to the existence of Dirac cones [21], graphene is known to exhibit intriguing transport properties, such as Klein tunneling, Zitterbewegung, anti-localization, abnormal quantum Hall effect, etc. Haldane et al. [22,23] pointed out the existence of photonic Dirac cones in two dimensional photonic crystals and discussed the unidirectional propagation of surface modes caused by the time-reversal symmetry breaking. Ochiai and Onada extended this discussion to honeycomb-lattice photonic crystals [24]. Zhang proposed the realization of Zitterbewegung effect in photonic crystals by the incidence of a pulse near the Dirac point frequency [25]. Pseudo-diffusive transmission with intensity inversely proportional to the thickness of photonic crystal array was also discovered by Sepkhanov et al. [16] and demonstrated by Diem et al. [26]. In the previous literatures, most of the Dirac conical dispersions are induced by the symmetry such as C_{6V}, C_{4V} and mirror symmetries, which can be understood by the theory of symmetry groups [13,14,27,28]. In the latest spotlights: breaking the symmetry has been utilized as a general method to destroy (gap) the Dirac points, and thus create band gaps supporting edge modes [12,29–36].

Accidental degeneracy in the band structure, which is a result of varying the material and geometrical parameters in the system, has also been utilized to realize some special band

#427389 https://doi.org/10.1364/OE.427389
Journal © 2021 Received 9 Apr 2021; revised 19 May 2021; accepted 19 May 2021; published 25 May 2021

Optics EXPRESS

dispersions. Huang et al. discovered that Dirac-like cone can be created at the center of the Brillouin zone by the accidental degeneracy of dipolar and monopolar bands in two-dimensional dielectric photonic crystals of square or triangular lattice [15]. At the Dirac-like point, such a system is equivalent to a material of zero effective refractive index [11,15,17,37–41]. Sakoda analyzed the creation of photonic Dirac-like cones by accidental degeneracy at the Brillouin zone center and some other high-symmetry points [13]. The Dirac-like points [12,15,41] or semi-Dirac points [38–40] have so far been realized on the high-symmetry lines or points in some symmetric systems. However, to date, the researches on the accidental degenerate points in systems without symmetry are still very limited.

In this paper, we introduce a general method to approximately create Dirac points and Dirac cones by accidental degeneracy in a system of photonic crystals without symmetry. This method is based on the band diagram engineering [42,43] which was utilized previously to enlarge the band gaps of photonic/phononic crystals. Here, we apply this engineering process to close up a band gap instead, which turns out to be a general and convenient way for the creation of Dirac cones of accidental degeneracy. To show the validity of this approach, we demonstrate three examples. In the first example, we break the high symmetry of the rod such that the Dirac cone at the K point of a triangular lattice is also broken, then we apply the band engineering (targeted insertions in the unit cell) to gradually close up the band gap and restore a Dirac cone in the system without symmetry. In the second example, we break the C_{6V} symmetry of a triangular lattice by changing the angle between the lattice vectors to be 45° instead of 60°, which also destroys the Dirac cone. Then, we apply the band engineering to the system and a Dirac cone is restored with this oblique lattice of 45°. Finally, in a photonic crystal of a square lattice, we demonstrate that Dirac cones can also be realized at a k point away from the high-symmetry lines and points. These findings reveal that the Dirac cones of accidental degeneracy can exist in general systems without symmetry. Furthermore, the Dirac cones of accidental degeneracy exhibit the same properties as the symmetry-induced Dirac cones, such as finite group velocity and pseudo-diffusive transmission. Our work thus paves a road for the realization of Dirac cones of accidental degeneracy in general systems without symmetry.

2. Method to create the Dirac cones of accidental degeneracy

The theory of band diagram engineering via the eigenmode analysis [42,43] is the foundation of this work. By analyzing the field distributions of the eigenmodes at the band edges, it is possible to change the unit structure of the photonic crystal accordingly, so as to shift the eigenfrequency towards the desired direction. For electromagnetic waves in two dimensional systems, the following formula has been obtained, respectively, for the transverse electric (TE) polarization (magnetic field polarized in the z direction) as

$$\left(\frac{\widetilde{\omega}_{nk}}{\omega_{nk}}\right)^2 - 1 \approx \frac{\int [\widetilde{\varepsilon}^{-1}(r) - \varepsilon^{-1}(r)]|D_{nk}(r)|^2 dr}{\int \varepsilon^{-1}(r)|D_{nk}(r)|^2 dr} \tag{1}$$

and for the transverse magnetic (TM) polarization (electric field polarized in the z direction) as

$$\left(\frac{\widetilde{\omega}_{nk}}{\omega_{nk}}\right)^2 - 1 \approx \frac{\int [\varepsilon(r) - \widetilde{\varepsilon}(r)]|E_{nk}(r)|^2 dr}{\int \varepsilon(r)|E_{nk}(r)|^2 dr} \tag{2}$$

Here, ω_{nk} and $\tilde{\omega}_{nk}$ denote the eigenfrequencies before and after the change of the unit structure, respectively. $\varepsilon(r)$ and $\varepsilon^{-1}(r)$ denote the permittivity distribution before and after the change of the unit structure, respectively. $D_{nk}(r)$ and $E_{nk}(r)$ denote the displacement and electric fields for the TE and TM cases, respectively. In the following, we utilize this theory to close up band gaps and create Dirac cones of accidental degeneracy.

Optics EXPRESS

In Fig. 1(a), we show the band diagram of the first two bands of a 2D triangular-lattice photonic crystal composed of dielectric rods with a diameter R=0.6a for the TM polarization. The lattice constant is a and the unit cell is shown in the inset graph. The dielectric rod and the background have permittivity 1 and 7, respectively. In the band diagram, it is clearly seen that there exists a Dirac point at the K point, due to the C_{6V} symmetry of the triangular lattice. Then, we break the high symmetry of the unit structure by changing the cylinder into a combination of a cylinder and a square column, as shown in the inset graph of Fig. 1(b). The degenerate Dirac point is thus broken and a band gap is formed between the two bands shown in Fig. 1(b). Next, we reduce this band gap and reform the Dirac point at the K point by using band diagram engineering, i.e. changing the unit structure according to the eigenfields of the band edge modes. From Eq. (2), for TM polarization, when $\varepsilon(r) - \tilde{\varepsilon}(r)>0$, i.e. the permittivity of the new structure is smaller than that of the original one, we have $(\tilde{\omega}_{nk}/\omega_{nk})^2>1$, i.e. the eigenfrequency would be shifted upward to higher frequencies. On the contrary, when $\varepsilon(r) - \tilde{\varepsilon}(r)<0$, i.e. the permittivity of the new structure is larger than that of the original one, we have $(\tilde{\omega}_{nk}/\omega_{nk})^2<1$ indicating that the eigenfrequency will be reduced. In order to close up the band gap and reform the Dirac point at the K point, the difference between the upper and the lower eigenfrequencies should be reduced. From Eq. (2), it is also seen that the effect of eigenfrequency shift is proportional to $|E_{nk}(r)|^2$, indicating that the modification of the unit structure should be made according to the distribution of the eigenfield $|E_{nk}(r)|^2$.

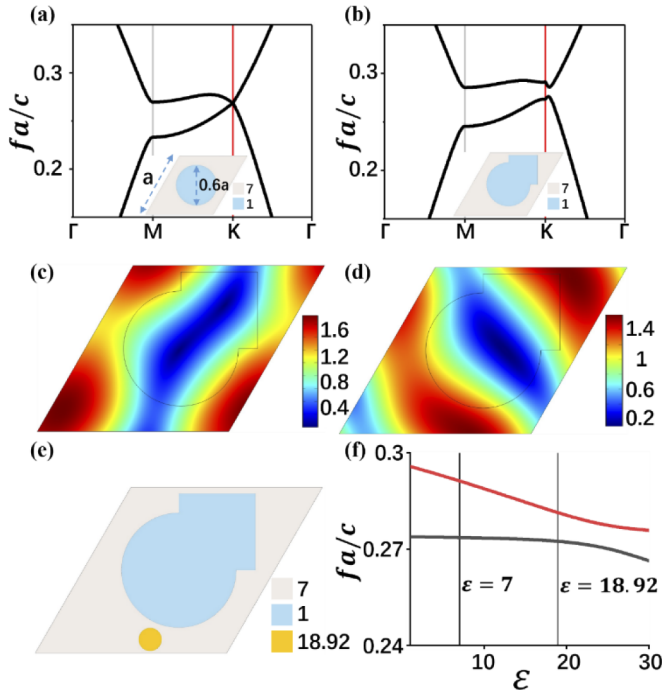

Fig. 1. (a) Band diagram for a triangular lattice of cylinders with a lattice constant a shown in the inset graph. The cylinder has a permittivity $\varepsilon = 1$ and diameter R=0.6a. The background has a permittivity $\varepsilon = 7$. (b) Band diagram after breaking the symmetry by changing the shape of the cylinder, as shown in the inset graph. (c) Distribution of $|E_z|$ at the K point of first band in Fig. 1(b). (d) Distribution of $|E_z|$ at the K point of second band in Fig. 1(b). (e) The engineering of the unit cell via an insertion of a rod with permittivity $\varepsilon = 18.92$. (f) Normalized frequencies of the two bands at the K point as functions of the permittivity of first inserted rod.

Optics EXPRESS

From the above analysis, in order to close up the band gap, the unit structure should be changed where the corresponding electric field intensity has the largest difference between the two eigenfields of the band edges. Therefore, two optimal ways to close up the gap are proposed here. One way is to shift the lower band edge of the band gap upward while keeping the upper edge almost intact. This can be achieved by reducing the permittivity where the field intensity is large for the eigenstate of lower frequency but small for that of the upper frequency; the other way is just the opposite. Here, Figs. 1(c) and (d) indicate the distribution of the electric field magnitude $|E_z|$ for the first and second bands at the K point of the Brillouin Zone. Considering the distinct difference between the two distributions, we insert a rod with a larger permittivity $\varepsilon = 18.92$ at the position shown in Fig. 1(e), where $|E_z|$ is nearly the minimum and the maximum in Figs. 1(c) and (d), respectively. Figure 1(f) shows how the normalized frequencies of the first two bands at the K point vary with the permittivity of the inserted new material. The black vertical line denotes the gap size before modification. The gray vertical line denotes the gap size after the insertion of a material with $\varepsilon = 18.92$. The comparison clearly shows that the band gap is decreased conspicuously after the insertion of the large permittivity. The gap size reaches the minimum at nearly $\varepsilon = 23$. However, here, in order to keep a feasible range of the permittivity, e.g. $1<\varepsilon<20$ at the infrared frequencies, we have chosen $\varepsilon = 18.92$ instead. As long as there exists a sufficient discrepancy between the distributions of the electric field intensity at the lower and upper band edges, we can always reduce the band gap until the gap becomes negligible and a Dirac point of accidental degeneracy is formed instead.

Figure 2(a) shows the optimized unit cell after a series of insertions of different materials. The different color squares denote different permittivities, while the vertical sequence of the squares denotes the order of insertion. More details of the engineering process are shown in the Supplement 1. Figure 2(b) shows the normalized frequency of the lower and upper band edges of the band gap at the K point, as a function of the permittivity of the last inserted rod (red circle in Fig. 2(a)). Clearly, the band gap decreases to near zero at $\varepsilon = 7.05$. Figure 2(c) shows the final

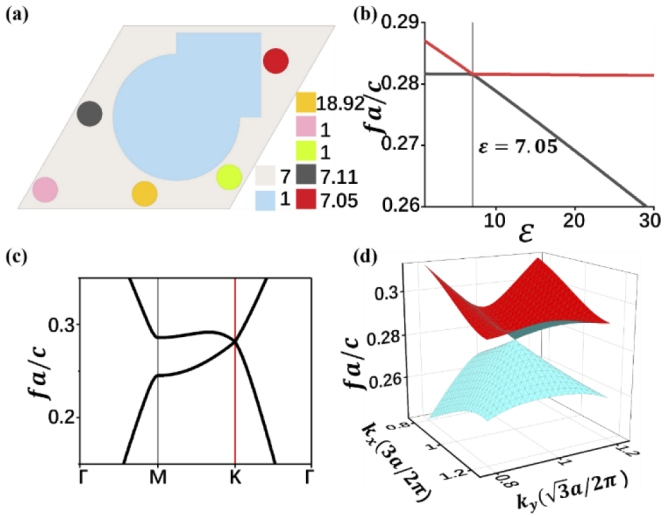

Fig. 2. (a) Optimized unit structure after a series of insertions of different materials. The different color squares denote different permittivities, while the vertical sequence of the squares denotes the order of insertion. (b) Normalized frequencies of the band edges at the K point as functions of the permittivity of last insertion. (c) Band diagram of the unit cell shown in Fig. 2(a). (d) Three-dimensional dispersion surfaces near the Dirac point frequency shown in Fig. 2(c).

Optics EXPRESS

band diagram of the optimized structure in Fig. 2(a), it can be clearly seen that the lower and upper band edges at the K point turns into a Dirac cone, just like the original Dirac cone due to the C_{6V} symmetry, as shown in Fig. 1(a). Figure 2(d) shows the three-dimensional dispersion surfaces near the Dirac point frequency shown in Fig. 2(c), which proves that a Dirac cone is formed with Dirac linear dispersions in the vicinity.

Another way to break the symmetry in Fig. 1(a) is to alter the lattice of the photonic crystals, e.g., by changing the angle between the lattice vectors to be 45° instead of 60°. This process breaks the C_{6V} symmetry of the triangular lattice. The band diagram is shown in Fig. 3(b), where the Dirac point is changed into a band gap at the K point. By applying the same method as discussed in Fig. 2, we show the optimized unit structure in Fig. 3(c). The different color squares denote different permittivities, while the vertical sequence of the squares denotes the order of insertion. In Fig. 3(d), we plot the band gap as a function of the permittivity of the last insertion. Clearly, the band gap is closed around ε = 7.1. The band diagram of the optimized structure is shown in Fig. 3(e), which demonstrates a reformed Dirac point at the K point due to the accidental degeneracy. This is also verified in Fig. 3(f), where the three-dimensional dispersion surfaces near the Dirac point frequency are plotted.

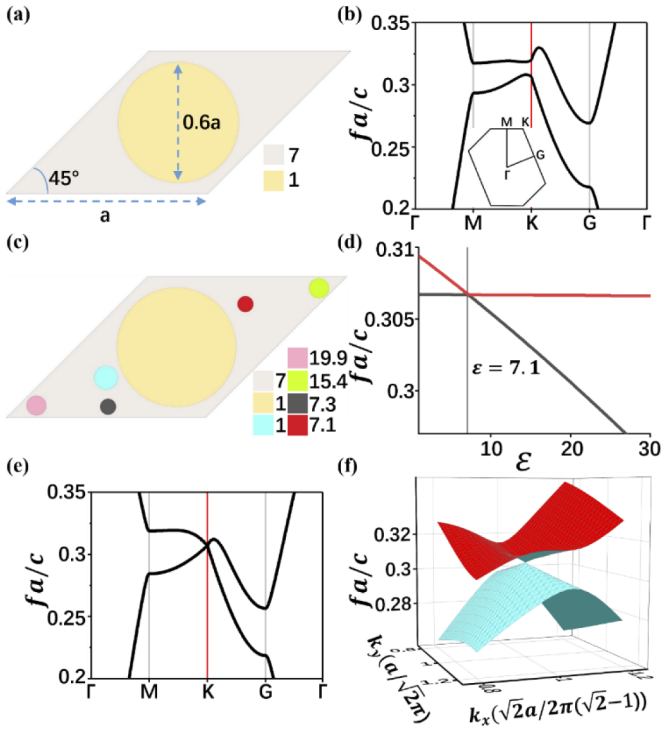

Fig. 3. (a) Breaking the C_{6V} symmetry of a triangular lattice by changing the angle between the lattice vectors to be 45°. The lattice constant is a. The cylinder has a permittivity ε = 1 and diameter R=0.6a. The background permittivity is ε = 7. (b) Band diagram of the unit cell shown in Fig. 3(a) with the first Brillouin zone shown in the inset graph. (c) Optimized unit structure after a series of insertions with different materials. The different color squares denote different permittivities, while the vertical sequence of the squares denotes the order of insertion. (d) Normalized frequencies of the band edges at the K point as functions of the permittivity of the last insertion. (e) Band diagram of the unit cell shown in Fig. 3(c). (f) Three-dimensional dispersion surfaces near the Dirac point frequency shown in Fig. 3(e).

Optics EXPRESS

In the above examples, the reformed Dirac points and Dirac cones are all located at the K point, which is a high-symmetry point in the Brillouin Zone. In fact, the position of the Dirac cones induced by accidental degeneracy is not limited to such high-symmetry points and lines. In the following, we demonstrate another example of the square lattice, and we create a Dirac point and a Dirac cone at a k point that is deviated from the high-symmetry lines or points. The unit cell of the original photonic crystal of a square lattice is shown in Fig. 4(a), the lattice constant is a and the side length of the square pillar is 0.5a. The dielectric constants of the pillar and the background are 7 and 1, respectively. Figure 4(b) shows the band diagram of the fourth and fifth bands. Here, the point G denotes a point along the XM line, with XG=1/3XM. Therefore, the line ΓG is inside the Brillouin Zone. Interestingly, we note that the lower and upper band edges of the band gap is nearly located on the line of the ΓG, as marked by the red line in Fig. 4(b). The inset graph shows the Brillouin Zone. In Fig. 4(c), we show the optimized structure after a series of insertions. The different color squares denote different permittivities, while the vertical sequence of the squares denotes the order of insertion. In Fig. 4(d), we plot the band gap as a function of the permittivity of the last insertion. Clearly, the band gap is closed around

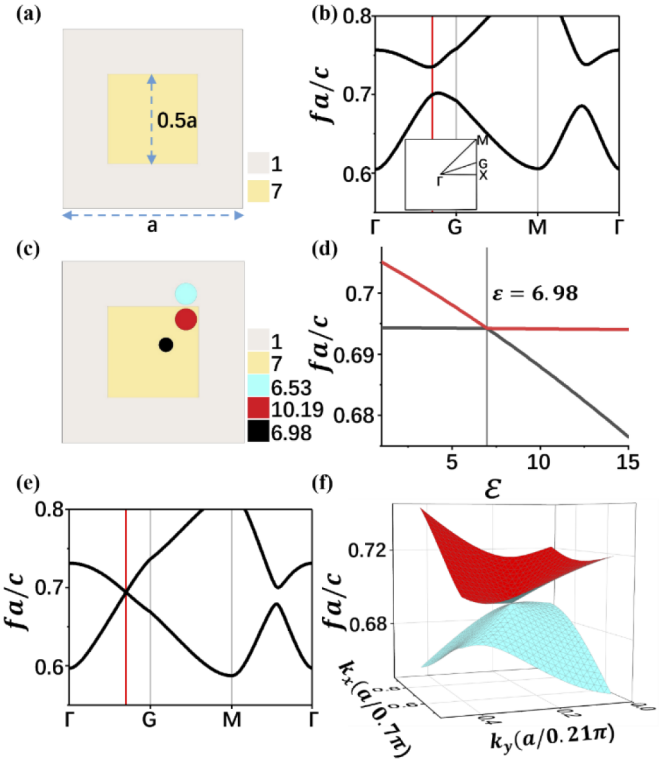

Fig. 4. (a) A square lattice of square pillars with a lattice constant a, side length L=0.5a and permittivity ε = 7.1 in a background with permittivity ε = 1. (b) Band diagram of the unit cell shown in Fig. 4(a) with first Brillouin zone shown in the inset graph. Here, the wave vector from the Γ point to a G point on the XM boundary is scanned. (c) Optimized unit structures after a series of insertions of different materials. The different color squares denote different permittivities, while the vertical sequence of the squares denotes the order of insertion. (d) Normalized frequencies of the band edges at a point along the ΓG direction as functions of the permittivity of the last insertion. (e) Band diagram of the unit cell shown in Fig. 4(c). (f) Three-dimensional dispersion surfaces near the Dirac point frequency shown in Fig. 4(e).

Optics EXPRESS

$\varepsilon = 6.98$. The band diagram of the optimized structure is shown in Fig. 4(e), which demonstrates a reformed Dirac point at the non-symmetry point, as induced by the accidental degeneracy. This is also verified in Fig. 4(f), where the three-dimensional dispersion surfaces near the Dirac point frequency are plotted.

3. Physical properties of the Dirac cones of accidental degeneracy

So far we have already demonstrated that Dirac points and Dirac cones can be induced by creating accidental degeneracy according to a systematic method of band diagram engineering. This method in principle works for arbitrary lattices and photonic crystals. In the following, we demonstrate that the Dirac cones of accidental degeneracy have the same unique physical properties as the symmetry-induced Dirac cones.

From the band diagrams and the three-dimensional dispersion surfaces shown in the corresponding models, we can straightly observe the linear dispersion relations near the Dirac cone as well as the degeneracy at the Dirac point. It is thus immediately inferred that such Dirac cones induced by accidental degeneracy also possess a finite group velocity, which is vitally important for the transmission of waves. It is well known that the Dirac conical dispersion would lead to many interesting phenomena, such as the Zitterbewegung effect [25] and pseudo-diffusive transmission [20,44]. It is thus beneficial to examine if the Dirac cones induced by accidental degeneracy also possess similar unique physical properties. Here, we focus on the pseudo-diffusive transmission that was previously demonstrated near the symmetry-induced Dirac cones [20,44]. Pseudo-diffusive transmission is a signature of the conical singularity. Near the Dirac point, the photon flux transmitted through a slab of photonic crystals is predicted to scale inversely proportional to the thickness of the slab, i.e. $G \sim 1/L$. The 1/L scaling is called "pseudo-diffusive" due to its reminiscence of the diffusion through a disordered medium, although here it appears for Bloch modes in the absence of any disorder inside the photonic crystals.

In order to verify the pseudo-diffusive transmission, we investigate the photonic crystal array with a width W and a thickness L, characterized as W×L. For the first model shown in Fig. 2(a), the frequency of the Dirac point is $f = 0.2827\omega a/2\pi c$. We consider a Gaussian wave incidence alone the ΓK direction onto the photonic crystals array, which is shown in Fig. 5(a) with a width of $W = 40\sqrt{3}a$. The photonic crystal array is about four times larger than the width of the Gaussian beam, so as to avoid the diffraction induced by the array boundary. The photon conductance G (the ratio between the total transmitted flux and incident photon flux) can be numerically obtained along the ΓK direction. In Fig. 5(b), we plot the calculated G×L as a function of the thickness L at $f = 0.285\omega a/2\pi c$ (near the Dirac point) in black square line. For comparison, the G×L at the frequencies $f = 0.25\omega a/2\pi c$ and $f = 0.23\omega a/2\pi c$ is also plotted in Fig. 5(b) in red circle line and blue triangle line, respectively. It can be seen clearly that at the frequency $f = 0.285\omega a/2\pi c$ near the Dirac point, G×L oscillates around a constant value. This indicates that the photon conductance is proportional to the inverse of array thickness, which is a signature of the pseudo-diffusive transmission near the frequency of the Dirac point. However, at the frequency $f = 0.23\omega a/2\pi c$, the photon conductance G remains a constant and G×L is a linearly ascending line with the array thickness L, i.e. the standard ballistic behavior characteristics. The case of frequency $f = 0.25\omega a/2\pi c$ is between the two cases of the previous frequencies.

We have also examined the case of the square lattice model shown in Fig. 4(c). The Dirac point is at the frequency $f = 0.694\omega a/2\pi c$. In this case, we consider an obliquely incident Gaussian wave with θ=9.68° onto the photonic crystals array shown in Fig. 5(c) with a width $W = 40\sqrt{3}a$. The incident angle is determined according to the wave vector of the Dirac point. Figure 5(d) shows the product G×L as a function of the array thickness at $f = 0.694\omega a/2\pi c$, $f = 0.692\omega a/2\pi c$ and $f = 0.681\omega a/2\pi c$, which is plotted in the black square line, red circle line

Optics EXPRESS

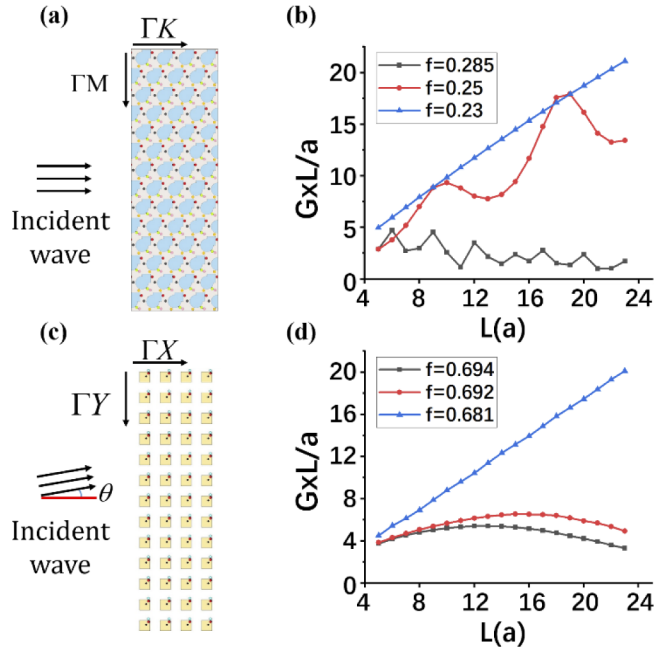

Fig. 5. (a) Schematic picture depicting the simulation process for the model shown in Fig. 2(a). (b) The product of G and L as a function of the array thickness L at different normalized frequencies shown with various colors and shapes. (c) Schematic picture depicting simulation processes for model shown in Fig. 3(c). (d) The product of G and L as a function of array thickness L at different normalized frequencies shown with various colors and shapes.

and blue triangle line, respectively. It can be seen clearly that the product G×L approximately remains a constant at the Dirac point frequency f = 0.694ωa/2πc as well as the frequency near the Dirac point f = 0.692ωa/2πc, which resemble the pseudo-diffusive transmission. While at the frequency f = 0.681ωa/2πc away from the frequency of the Dirac point, the photon conductance G remains a constant with the increase of thickness L, indicating a ballistic behavior in stark contrast to the pseudo-diffusive behavior. Therefore, it is proved that the Dirac cones induced by symmetry and accidental degeneracy exhibit the same characteristics. The Dirac cones formed in the systems without symmetry also support the same physical effect as previously observed for the Dirac cones in systems with C_{6V}, C_{4V} and mirror symmetries. We note that the observation of the diffusive transmission is a signature of the conical dispersion in the vicinity of a near-perfect degeneracy point.

4. Summary

Our method signifies that symmetries are not indispensable for the creation of Dirac points and Dirac cones. Based on the approach of engineering accidental degeneracy, it is possible to turn a band gap into a Dirac point and a Dirac cone, which were previously associated with the high symmetries such as C_{6V}, C_{4V} and mirror symmetries. Therefore, our work indicates that the physics related to Dirac cones can be extended to systems without symmetry.

In normal systems without symmetry, the anti-crossing phenomenon prevents the realization of accidental degeneracy. Actually, in each step of our band engineering process, we have also observed the anti-crossing phenomenon, as is shown in the Supplement 1. For each insertion, tuning its parameter can reduce the band gap, but there is a minimal gap induced by the anti-crossing. Interestingly, a new insertion can always be designed to further reduce the

Optics EXPRESS

band gap beyond the previous minimal gap. By adding an infinite number of insertions, the band gap in principle can eventually become infinitesimal, i.e. achieving the accidental degeneracy. At the occurrence of degeneracy, the orthogonality between the eigenstates is not protected by symmetry, but induced by the series of modification made to the photonic system according to the eigenstates.

Comparing with the previous Dirac-like cones induced by accidental degeneracy that exhibit additional flat bands [15], the Dirac cones obtained here is free of the flat dispersions and thus is more similar to the Dirac cones extensively discussed in Graphene *et al*. We note that the previous Dirac-like cone requires the system to have the C_{6V} or C_{4V} symmetry, otherwise the Dirac-like point would turn into the semi-Dirac point at the accidental degeneracy [45]. This stringent demand in symmetry is removed in our system. Moreover, unlike the previous Dirac-like cone at the Brillouin Zone center, here the Dirac cone is not limited to the Brillouin Zone center, or any high symmetry points or lines, and can in principle appear at any place inside the Brillouin Zone. This attributes to the accidental degeneracy in the designed photonic crystal without symmetry. The free position of the Dirac cone beyond the high symmetry points and lines in the Brillouin Zone can provide more degrees of freedoms for the Dirac cone physics.

It has been found that accidental degeneracy is sometimes associated with the so-called hidden symmetry [46,47], which is mathematically defined in the Hamiltonian model of the system near the degeneracy point. Here, the symmetry of photonic crystals refers to more common space symmetries, such as the rotational symmetry, mirror symmetry, etc. The photonic crystals demonstrated here have only periodicity and no other space symmetries.

In conclusion, we have created Dirac cones at different k points in the reciprocal space by designing photonic crystals without symmetry. The degeneracy in the Dirac point is formed by an accidental set of system parameters, which can be obtained through a method of band diagram engineering according to the eigenstates. Under such circumstances, Dirac conical dispersions are formed around the Dirac point, which extends the important physics of Dirac conical dispersions to more general systems without symmetry.

Funding. National Key Research and Development Program of China (2017YFA0303702, 2020YFA0211300); National Natural Science Foundation of China (11634005, 11974176, 11974177, 61671314, 61975078).

Disclosures. The authors declare no conflicts of interest.

Data availability. Data underlying the results presented in this paper are not publicly available at this time but maybe obtained from the authors upon reasonable request.

Supplemental document. See Supplement 1 for supporting content.

References

1. D. Malko, C. Neiss, F. Viñes, and A. Görling, "Competition for Graphene: Graphynes with Direction-Dependent Dirac Cones," Phys. Rev. Lett. **108**(8), 086804 (2012).
2. Y. Zhang, Y.-W. Tan, H. L. Stormer, and P. Kim, "Experimental observation of the quantum Hall effect and Berry's phase in graphene," Nature **438**(7065), 201–204 (2005).
3. V. P. Gusynin and S. G. Sharapov, "Unconventional Integer Quantum Hall Effect in Graphene," Phys. Rev. Lett. **95**(14), 146801 (2005).
4. P. A. M. Dirac and R. H. Fowler, "The quantum theory of the electron," Proc. SPIE **117**(778), 610–624 (1928).
5. Q. Guo, O. You, B. Yang, J. B. Sellman, E. Blythe, H. Liu, Y. Xiang, J. Li, D. Fan, J. Chen, C. T. Chan, and S. Zhang, "Observation of Three-Dimensional Photonic Dirac Points and Spin-Polarized Surface Arcs," Phys. Rev. Lett. **122**(20), 203903 (2019).
6. C. Hu, Z. Li, R. Tong, X. Wu, Z. Xia, L. Wang, S. Li, Y. Huang, S. Wang, B. Hou, C. T. Chan, and W. Wen, "Type-II Dirac Photons at Metasurfaces," Phys. Rev. Lett. **121**(2), 024301 (2018).
7. Q. Guo, B. Yang, L. Xia, W. Gao, H. Liu, J. Chen, Y. Xiang, and S. Zhang, "Three Dimensional Photonic Dirac Points in Metamaterials," Phys. Rev. Lett. **119**(21), 213901 (2017).
8. C. Xu, H. Chu, J. Luo, Z. Hang, Y. Wu, and Y. Lai, Three-dimensional Electromagnetic Void Space (2020).
9. G.-G. Liu, P. Zhou, Y. Yang, H. Xue, X. Ren, X. Lin, H.-x. Sun, L. Bi, Y. Chong, and B. Zhang, "Observation of an unpaired photonic Dirac point," Nat. Commun. **11**(1), 1873 (2020).

Optics EXPRESS

10. M. Milićević, G. Montambaux, T. Ozawa, O. Jamadi, B. Real, I. Sagnes, A. Lemaître, L. Le Gratiet, A. Harouri, J. Bloch, and A. Amo, "Type-III and Tilted Dirac Cones Emerging from Flat Bands in Photonic Orbital Graphene," Physical Review X **9**, 031010 (2019).
11. M. Minkov, I. A. D. Williamson, M. Xiao, and S. Fan, "Zero-Index Bound States in the Continuum," Phys. Rev. Lett. **121**(26), 263901 (2018).
12. W.-Y. He and C. T. Chan, "The Emergence of Dirac points in Photonic Crystals with Mirror Symmetry," Sci. Rep. **5**(1), 8186 (2015).
13. K. Sakoda, "Universality of mode symmetries in creating photonic Dirac cones," J. Opt. Soc. Am. B **29**(10), 2770–2778 (2012).
14. C.-T. Chan, X. Huang, F. Liu, and Z. Hang, "Dirac Dispersion and Zero-Index in Two Dimensional and Three Dimensional Photonic and Phononic Systems (Invited Paper)," Prog. Electromagn. Res. B **44**, 163–190 (2012).
15. X. Huang, Y. Lai, Z. H. Hang, H. Zheng, and C. T. Chan, "Dirac cones induced by accidental degeneracy in photonic crystals and zero-refractive-index materials," Nat. Mater. **10**(8), 582–586 (2011).
16. R. A. Sepkhanov, Y. B. Bazaliy, and C. W. J. Beenakker, "Extremal transmission at the Dirac point of a photonic band structure," Phys. Rev. A **75**(6), 063813 (2007).
17. C. Xu, G. Ma, Z.-G. Chen, J. Luo, J. Shi, Y. Lai, and Y. Wu, "Three-Dimensional Acoustic Double-Zero-Index Medium with a Fourfold Degenerate Dirac-like Point," Phys. Rev. Lett. **124**(7), 074501 (2020).
18. Y. Li, Y. Wu, and J. Mei, "Double Dirac cones in phononic crystals," Appl. Phys. Lett. **105**(1), 014107 (2014).
19. F. Liu, Y. Lai, X. Huang, and C. T. Chan, "Dirac cones at $\vec{k} = 0$ in phononic crystals," Phys. Rev. B **84**(22), 224113 (2011).
20. X. Zhang and Z. Liu, "Extremal Transmission and Beating Effect of Acoustic Waves in Two-Dimensional Sonic Crystals," Phys. Rev. Lett. **101**(26), 264303 (2008).
21. A. H. Castro Neto, F. Guinea, N. M. R. Peres, K. S. Novoselov, and A. K. Geim, "The electronic properties of graphene," Rev. Mod. Phys. **81**(1), 109–162 (2009).
22. S. Raghu and F. D. M. Haldane, "Analogs of quantum-Hall-effect edge states in photonic crystals," Phys. Rev. A **78**(3), 033834 (2008).
23. F. D. M. Haldane and S. Raghu, "Possible Realization of Directional Optical Waveguides in Photonic Crystals with Broken Time-Reversal Symmetry," Phys. Rev. Lett. **100**(1), 013904 (2008).
24. T. Ochiai and M. Onoda, "Photonic analog of graphene model and its extension: Dirac cone, symmetry, and edge states," Phys. Rev. B **80**(15), 155103 (2009).
25. X. Zhang, "Observing Zitterbewegung for Photons near the Dirac Point of a Two-Dimensional Photonic Crystal," Phys. Rev. Lett. **100**(11), 113903 (2008).
26. M. Diem, T. Koschny, and C. M. Soukoulis, "Transmission in the vicinity of the Dirac point in hexagonal photonic crystals," Phys. B **405**(14), 2990–2995 (2010).
27. J. Mei, Y. Wu, C. T. Chan, and Z.-Q. Zhang, "First-principles study of Dirac and Dirac-like cones in phononic and photonic crystals," Phys. Rev. B **86**(3), 035141 (2012).
28. K. Sakoda, "PHOTONIC DIRAC CONES REALIZED BY ACCIDENTAL DEGENERACY ON THE BRILLOUIN-ZONE BOUNDARY," Int. J. Mod. Phys. B **28**(02), 1441008 (2014).
29. Y. Liu, S. Leung, F.-F. Li, Z.-K. Lin, X. Tao, Y. Poo, and J.-H. Jiang, "Bulk–disclination correspondence in topological crystalline insulators," Nature **589**(7842), 381–385 (2021).
30. M. Makwana, R. Craster, and S. Guenneau, "Topological beam-splitting in photonic crystals," Opt. Express **27**(11), 16088–16102 (2019).
31. B. Xia, G. Wang, and S. Zheng, "Robust edge states of planar phononic crystals beyond high-symmetry points of Brillouin zones," J. Mech. Phys. Solids **124**, 471–488 (2019).
32. Y. Yang, Z. Gao, X. Feng, Y.-X. Huang, P. Zhou, S. A. Yang, Y. Chong, and B. Zhang, "Ideal Unconventional Weyl Point in a Chiral Photonic Metamaterial," Phys. Rev. Lett. **125**(14), 143001 (2020).
33. T. Ozawa, H. M. Price, A. Amo, N. Goldman, M. Hafezi, L. Lu, M. C. Rechtsman, D. Schuster, J. Simon, O. Zilberberg, and I. Carusotto, "Topological photonics," Rev. Mod. Phys. **91**(1), 015006 (2019).
34. A. Slobozhanyuk, S. H. Mousavi, X. Ni, D. Smirnova, Y. S. Kivshar, and A. B. Khanikaev, "Three-dimensional all-dielectric photonic topological insulator," Nat. Photonics **11**(2), 130–136 (2017).
35. L. Lu, C. Fang, L. Fu, S. G. Johnson, J. D. Joannopoulos, and M. Soljačić, "Symmetry-protected topological photonic crystal in three dimensions," Nat. Phys. **12**(4), 337–340 (2016).
36. L. Lu, J. D. Joannopoulos, and M. Soljačić, "Topological photonics," Nat. Photonics **8**(11), 821–829 (2014).
37. T. Dong, J. Liang, S. Camayd-Muñoz, Y. Liu, H. Tang, S. Kita, P. Chen, X. Wu, W. Chu, E. Mazur, and Y. Li, "Ultra-low-loss on-chip zero-index materials," Light: Sci. Appl. **10**(1), 10 (2021).
38. M. Dubois, C. Shi, X. Zhu, Y. Wang, and X. Zhang, "Observation of acoustic Dirac-like cone and double zero refractive index," Nat. Commun. **8**(1), 14871 (2017).
39. Y. Li, S. Kita, P. Muñoz, O. Reshef, D. I. Vulis, M. Yin, M. Lončar, and E. Mazur, "On-chip zero-index metamaterials," Nat. Photonics **9**(11), 738–742 (2015).
40. P. Moitra, Y. Yang, Z. Anderson, I. I. Kravchenko, D. P. Briggs, and J. Valentine, "Realization of an all-dielectric zero-index optical metamaterial," Nat. Photonics **7**(10), 791–795 (2013).
41. F. Liu, X. Huang, and C. T. Chan, "Dirac cones at k→=0 in acoustic crystals and zero refractive index acoustic materials," Appl. Phys. Lett. **100**(7), 071911 (2012).

Optics EXPRESS

42. X. Zhang, Z.-Q. Zhang, L.-M. Li, C. Jin, D. Zhang, B. Man, and B. Cheng, "Enlarging a photonic band gap by using insertion," Phys. Rev. B **61**(3), 1892–1897 (2000).
43. C. Xu, G. Wang, Z. H. Hang, J. Luo, C. T. Chan, and Y. Lai, "Design of full-k-space flat bands in photonic crystals beyond the tight-binding picture," Sci. Rep. **5**(1), 18181 (2015).
44. X. Zhang, "Demonstration of a new transport regime of photon in two-dimensional photonic crystal," Phys. Lett. A **372**(19), 3512–3516 (2008).
45. Y. Wu, "A semi-Dirac point and an electromagnetic topological transition in a dielectric photonic crystal," Opt. Express **22**(2), 1906–1917 (2014).
46. J.-M. Hou and W. Chen, "Hidden antiunitary symmetry behind "accidental" degeneracy and its protection of degeneracy," Front. Phys. **13**(1), 130301 (2018).
47. R. Lemus, A. Frank, M. V. Andrés, and F. Leyvraz, "Accidental degeneracy and hidden symmetry: Rectangular wells with commensurate sides," Am. J. Phys. **66**(7), 629–631 (1998).